Stacking and band structure of van der Waals bonded graphane multilayers

Jochen Rohrer[1,*] and Per Hyldgaard[1]

[1] *BioNano Systems Laboratory, Department of Microtechnology, MC2, Chalmers University of Technology, SE-412 96 Gothenburg*

(Dated: October 14, 2010)

We use density functional theory and the van der Waals density functional (vdW-DF) method to determine the binding separation in bilayer and bulk graphane and study the corresponding electronic band structure. The calculated binding separation (distance between center-of-mass planes) and binding energy are $4.5-5.0$ Å ($4.5-4.8$ Å) and $75-102$ meV/cell ($93-127$ meV/cell) in the bilayer (bulk), depending on the choice of vdW-DF version. We obtain the corresponding band diagrams using ordinary GGA calculations for the geometries specified by our vdW-DF results. We find significant band-gap modifications by up to -1.2 eV (+4.0 eV) in various regions of the Brillouin zone, produced by the bilayer (bulk) formation. The possibility of such large modifications signals a potential of vdW-induced band-gap engineering in other materials

PACS numbers: 81.05.U-,73.22.Pr,71.15.Mb

I. INTRODUCTION

Selective modification of band gaps (band-gap engineering) by atomic-scale design of materials is a powerful concept in electronic and photonic development.[1] Band gaps can be altered by, for example, introducing dopants, defects, or by exploiting finite size effects.[2,3] The physical origin of band gap variations is a modification in the charge distribution in concert with wavefunction hybridization and modification.

Dispersive or van der Waals (vdW) interactions[4] also alter the distribution of electronic charges. This is evident, for example, by considering the formation of the double-dipole configuration[5] which is the electrostatic signature and inherent nature of a pure vdW binding.[4,5] In addition, there are also geometry-induced effects of the vdW binding on electron behavior. For example, vdW-binding can cause smaller amounts of net charge transfer within individual vdW-bonded fragments.[6] Also, wavefunction hybridization will certainly arise when materials fragments approach one another, even if this hybridization does not significantly contribute to the binding itself (in purely dispersive interaction). Wavefunction hybridization and Pauli exclusion cause scattering of the surface-state electrons in physiosorption of acenes and quinones on Cu(111), even if there is no net charge transfer.[7,8] It is therefore important to quantify the extent to which van der Waals (vdW) bonding can modify the electron dispersion, that is, the band-structure. Such a study is now possible, since recent development of the vdW density functional (vdW-DF) method[5,9–11] enables systematic (theoretical) explorations of bonding in sparse materials within density functional theory (DFT).[4]

In this paper we investigate geometry-induced effects on electronic structure. In particular we separately study the effects of (1) the enhanced charge density in regions where the tails of vdW-bonded material fragments overlap, see left panel of Fig. 1, (2) the hybridization of wave functions, and (3) the redistribution of charge density due to mechanisms that are not inherent to the vdW interaction (such as local displacements due to electrostatics and Pauli-repulsion), see right panel of Fig. 1.

We focus on the band structure of layered systems of the macromolecule graphane,[12,13] a fully hydrogenated derivative of graphene.[14] The top panel of Fig. 2 shows the atomic structure of (the stable chair conformation of) monolayer (ML) graphane, consisting of a (slightly buckled) graphene backbone with H atoms attached in alternating fashion above and below the carbon plane. Bilayer graphane with possible high-symmetry structure shown in the bottom panels of Fig. 2 present a possible new system.[15,16] In addition, we also include a study of

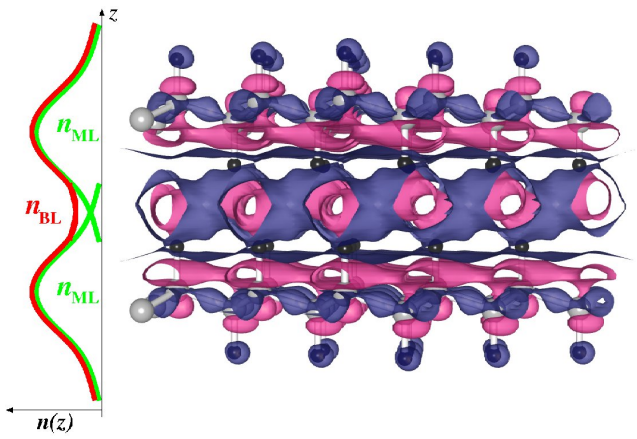

FIG. 1: (Color) Charge density in vdW-bonded graphane bilayers. The left panel shows a schematics of the non-selfconsistent bilayer (BL) charge density obtained by adding two monolayer (ML) densities and resulting into a charge enhancement in the interlayer region. The right panel depicts calculated self-consistent (on the GGA level) charge rearrangements. Our Bader analysis[19,20] shows that the charge rearrangements are *not* accompanied by any significant net charge transfer into the middle region. Color coding: light large spheres represent C atoms, black small spheres represent H atoms; accumulation of charge is indicated by the pink (light) isosurface, depletion by the purple (dark) isosurface.

a possible bulk graphane crystal.

Graphane adds to the wealth of carbon-based materials that are considered as promising materials for near-future nanoelectronic devices.[17,18] Pure graphene has a zero band gap and extraordinary conduction properties. Electronic devices, however, also require semiconducting and insulating materials. Such materials can be obtained from pure graphene as derivatives either in the form of graphene nanoribbons[21,22] or by chemical modification through adsorbates.[23,24] Monolayer graphane belongs to the last-mentioned group of derivatives. DFT calculations predict a large band-gap semiconductor nature;[12] the more advanced GW method[25] predicts an insulating nature.[26] Graphane has been proposed theoretically to serve as natural host for graphene quantum dots[27] or graphene nanoribbons for nanoroads.[28] Furthermore, doped graphane has been recently predicted to be a high-T_c superconductor.[29] Such potential application of the graphane structure makes it interesting to explore possibilities to (locally) modify the the electronic behavior either by selective hydrogen removal[26–28] or by geometry-induced band-structure modifications.

The paper is organized as follows. In Sec. II, we give a survey of all considered high-symmetry graphane bilayer configurations. Section III presents our computational method. In Sec. IV, we present, analyze and discuss our results. Section VII summarizes our work and contains our conclusions.

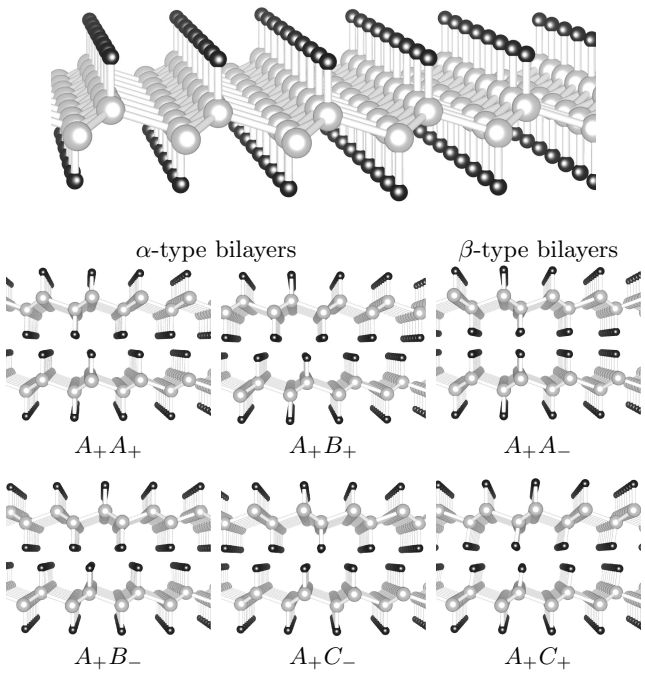

FIG. 2: Structure of monolayer (top panel) graphane and of high-symmetry graphane bilayer (BL) configurations. The labeling $(A_+A_-, \dots)$ provides an unambiguous and exhaustive identification of all high-symmetry atomic configurations for the BL system as explained in the text. Light large spheres represent C atoms, black small spheres represent H atoms.

II. HIGH-SYMMETRY GRAPHANE BILAYERS

The set of lower panels in Fig. 2 shows all six high-symmetry arrangements of bilayer (BL) graphane. These can be grouped into two different types. In α-type BL, the graphane sheets are interlocked with each other. In β-type BL, the H atoms from different graphane sheets (located between the sheets) sit on top of each other. We calculate and compare all of these configurations that make up the α- and β-type sets of stacking configurations.

The set of different (high-symmetry) arrangements for the BL systems are found as follows. We label the sheets according to the location of vacancy in the C backbone in the unit cell (A, B, or C sites). In addition, the distortion of the C backbone along the z-direction (+ or −) of the first occupied C site (counted along the main diagonal starting from the vacancy stacking) is indicated as a subscript label. In all BL, the first layer can be arbitrarily chosen to be an A_+ layer. The second layer is placed on top of the first one of the following actions: (i) copying the bottom layer and moving it along the z-direction (A_+A_+); (ii) flipping the bottom layer and moving it along the z-direction (A_+A_-); (iii) as in (i) and additionally moving it along the long diagonal of the 2D graphane lattice by one third (A_+B_+); (iv) as (ii) and additionally moving it along the long diagonal of the 2D graphane lattice by one third (A_+B_-); (v) as in (i) and additionally moving it along the long diagonal of the 2D graphane lattice by two thirds (A_+C_+); (vi) as in (ii) and additionally moving it along the long diagonal of the 2D graphane lattice by two thirds (A_+C_-).

III. COMPUTATIONAL METHOD

A. vdW binding

We map out the energy variation of bilayer (bulk) graphane as a function of the separation between two graphane sheets (the c-parameter of the bulk unit cell) using (non-selfconsistent) vdW-DF calculations. For BL, we employ supercells with our optimized 1×1 graphane in-plane lattice parameters [$a_1 = (a, 0, 0)$, $a_2 = (a/2, \sqrt{3}/2 \cdot a, 0)$ with $a = 2.532$] and a height of 30 Å. For the bulk, we optimize the c-parameter of the periodic unit cell [$a_3 = (0, 0, c)$] starting from the optimal value of the BL separation.

Our calculations combine selfconsistent GGA-DFT calculations with three (non-selfconsistent) versions of the vdW-DF method. The GGA calculations are performed with the planewave pseudopential[30] code Dacapo,[31] using PBE[32] for exchange and correlation. We use a planewave cutoff of 500 eV and a 4×4×1 (4×4×2) k-point sampling[33]. The three versions of the vdW-

DF method that we use are (i) the nonlocal correlation functional of *Dion et al.*[9] in conjunction with revPBE[34] for exchange (vdW-DF1), (ii) the same correlation functional but with the exchange part of the C09 functional[11] (vdW-DF1-C09$_x$), and (iii) the most recent version of the vdW-DF method, Ref. 10 (vdW-DF2). The latter version uses the refitted form of the PW86 functional (rPW86$_x$)[35] for exchange. We obtain total energies as

$$E^{\text{vdW-DF}}[n] = E_0[n] + E_c^{\text{nl}}[n]. \quad (1)$$

Here, $E_c^{\text{nl}}[n]$ is the energy obtained from one of the nonlocal functionals of Refs. 9 and 10, and $E_0[n]$ is given by

$$E_0 = E_{\text{tot}}^{\text{PBE}} - E_{\text{xc}}^{\text{PBE}} + E_c^{\text{VWN}} + E_x^{\text{v}}. \quad (2)$$

where E_c^{VWN} is the VWN-LDA[36] correlation energy and the subscript 'v' denotes the version of the exchange functional (revPBE$_x$, C09$_x$, or rPW86$_x$). We define the layer binding energy as

$$E_{\text{bind}}(d_{\text{cmp}}) = E_{\text{vdW-DF}}(d_{\text{cmp}}) - E_{\text{vdW-DF}}(d_{\text{cmp}} \to \infty). \quad (3)$$

Here, d_{cmp} is the distance between the center-of-mass planes in each graphane sheet of the monolayer.

Our numerical evaluation of Eq. (3) proceeds in the same way as described in Refs. 7 and 37–40. In particular, because of a small but nonnegligible sensitivity of the nonlocal correlation on the exact positioning of atoms with respect to the density grid, we avoid a direct comparsion of $E_c^{\text{nl}}[n]$ for BL configurations with different ML separations. Instead we evaluate the layer-binding energy by comparing changes in the nonlocal correlation arising between the actual configuration and a reference that keeps the same alignment of atoms and grid points. Specifically, for all configurations we evaluate the change in nonlocal correlation as $\Delta E_c^{\text{nl}}[n] = E_{c,\,\text{PQ}}^{\text{nl}}[n] - E_{c,\,\text{P}}^{\text{nl}}[n] - E_{c,\,\text{Q}}^{\text{nl}}[n]$. Here $E_{c,\,\text{PQ}}^{\text{nl}}[n]$ is the nonlocal correlation energy of the full BL configuration (with one ML in P and one in Q) and $E_{c,\,\text{P}}^{\text{nl}}[n]$ ($E_{c,\,\text{Q}}^{\text{nl}}[n]$) is the nonlocal energy of the configuration where one ML has been removed from Q (P) while the other is kept at precisely the same location P (Q) as in the BL configuration. Further details on our approach to increase the accuracy of vdW-DF are provided in Refs. 7 and 37.

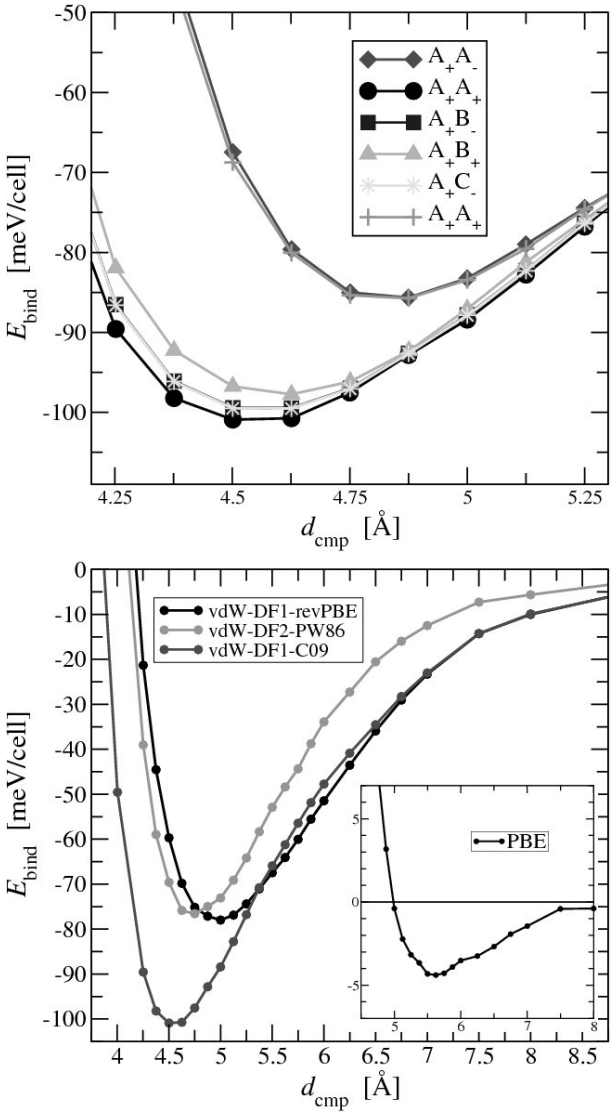

FIG. 3: Calculated layer-binding energy variations as functions of the center-of-mass (cmp) separation d_{cmp} between two graphane sheets. The top panel compares energy variations of the six different high-symmertry graphane configurations calculated with vdW-DF1-C09$_x$. The α-type bilayer have in general lower energy than β-type configurations. The A_+A_+ on-top configuration shows the strongest binding. The bottom panel compares the different version of vdW-DF for the A_+A_+ configuration. All versions of vdW-DF predict qualitatively the same energy variations but the detailed numerical values of the binding separations and energies vary. The insert emphasizes that GGA calculations provide no meaningful account of the binding.

B. Band structure

We determine the band-structures with pure non-selfconsistent GGA calculations for various k points. We fix the BL separation (bulk c-parameter) to the value calculated with vdW-DF. The selfconsistent input density for these non-selfconsistent band-structure calculations is obtained using a planewave cutoff of 500 eV and a 20×20×1 (20×20×5) k-point sampling[33] for the bilayer (bulk).

For the bilayer, the Brillouin zone (BZ) is two-dimensional and relevant k points are $\Gamma = (0,0,0)$, $\text{K} = (2/3,1/3,0)$ and $\text{M} = (1/2,1/2,0)$.[41] All special points are given in units of the reciprocal lattice vectors. We calculate the band variations along the paths $\overline{\text{K}\Gamma}$, $\overline{\Gamma\text{M}}$, and $\overline{\text{KM}}$.

For the bulk, the BZ is three-dimensional. Therefore

	bilayer graphane		
	vdW-DF1	vdW-DF2	vdW-DF1-C09$_x$
d_{cmp} [Å]	5.0	4.75	4.5
E_{bind} [meV/cell]	78	77	101
E_{gap} at Γ [eV]	3.46 (-0.08)	3.53 (-0.01)	3.61 (+0.07)
E_{gap} at K [eV]	11.86 (-0.30)	11.75 (-0.41)	11.61 (-0.55)
E_{gap} at M [eV]	10.40 (-0.46)	10.31 (-0.55)	10.24 (-0.62)
	bulk graphane		
	vdW-DF1	vdW-DF2	vdW-DF1-C09$_x$
c [Å]	4.8	4.7	4.5
E_{bind} [meV/cell]	93	94	127
E_{gap} at Γ [eV]	7.23 (+3.69)	7.50 (+3.96)	8.01 (+4.47)
E_{gap} at K [eV]	12.77 (+0.61)	12.83 (+0.67)	12.66 (+0.50)
E_{gap} at M [eV]	10.00 (-0.86)	9.95 (-0.91)	9.85 (-1.01)
E_{gap} at A [eV]	3.52 (-0.02)	3.62 (+0.08)	3.88 (+0.34)
E_{gap} at H [eV]	11.63 (-0.53)	11.58 (-0.58)	11.48 (-0.68)
E_{gap} at L [eV]	11.27 (+0.41)	11.27 (+0.41)	11.28 (+0.42)

TABLE I: Binding separations d_{cmp} (the c- lattice parameter) layer-binding energies energies E_{bind}, and band gaps E_{gap} at several k points in the Brillouin zone of bilayer (bulk) graphane. All quantities are calculated with three versions of vdW-DF. For the band gaps, the difference with respect to a graphane monolayer are given in parentheses [a negative value corresponds to a decreased band gap in the bilayer (bulk)].

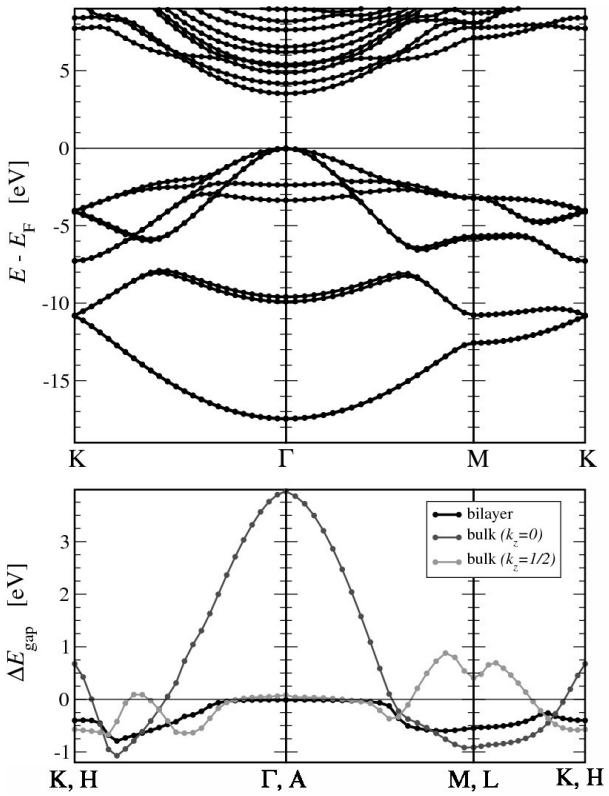

FIG. 4: Electronic band structure of bilayer (BL) and bulk graphane. The top panel shows the overall band diagram along $\overline{\mathrm{K\Gamma}}$, $\overline{\Gamma\mathrm{M}}$, and $\overline{\mathrm{MK}}$ of a A_+A_+ BL at the binding separation predicted by vdW-DF2. Apart from the fact that each band exists as a pair of bands, the BL band-structure qualitatively agrees with that of of a monolayer (ML, see Fig. 3 in Ref. 12). The bottom panel shows the k-dependent (direct) band-gap variation in the BL and bulk with respect to the band-gap variation in the ML. For the bulk, we also show the band-gap variation along $\overline{\mathrm{HA}}$, $\overline{\mathrm{AL}}$, and $\overline{\mathrm{LH}}$. In the BL, at and around the Γ point, the gap is essentially unchanged. However, away from the Γ point significant band-gap reduction is observed. In the bulk, local band-gap modifications can be both positive and negative and their absolute can be even larger than in the BL. The calculated band-gap modifications indicate a potential for exploiting vdW interactions in band gap engineering.

non-zero values of k_z are important and we also calculate the band variations along $\overline{\mathrm{HA}}$, $\overline{\mathrm{AL}}$, and $\overline{\mathrm{LH}}$. Here, the special points are A $= (0, 0, 1/2)$, H $= (2/3, 1/3, 1/2)$, and L $= (1/2, 1/2, 1/2)$.[41]

IV. RESULTS: PREDICTED PROPERTIES OF BILAYER AND BULK GRAPHANE

Figure 3 shows the calculated variations in layer-binding energy as functions of the separation between the center-of-mass planes ('cmp') of the two graphane monolayers (ML) in a bilayer (BL). The top panel compares the energy variations for the configurations with different stackings using vdW-DF1-C09$_x$. The energy variations split according to the grouping into α- and β-type configurations. The α-type configurations have a smaller binding separation and a higher binding energy; the A_+A_+ stacking shows the strongest bonding.

The bottom panel compares the energy variations of the A_+A_+ BL for vdW-DF1, vdW-DF1-C09$_x$, and vdW-DF2. Qualitatively, all functionals yield the same energy variations. The insert shows the energy variation for the A_+A_+ configuration obtained from pure PBE calculations and illustrates that no meaningful binding is predicted without an account of vdW forces.

Table I lists and compares numerical results for the calculated binding separations and layer-binding energies for the BL. The binding separations and energies range from 4.5 Å to 5.0 Å and 75 meV/cell to and 102 meV/cell, depending on the version of vdW-DF. The binding energy is comparable to that in a graphene BL[42] (94 meV using vdW-DF1).

Table I also lists the calculated lattice constant c and the corresponding layer-binding energies for a fictitious bulk crystal of graphane. It is possible that such a 3D graphane system might eventually be synthesized. We here present predictions of the expected structure, using our analysis of stacking in the BL as starting point. In particular we focus on A_+A_+ stacking and find that the lattice constant essentially coincides with d_{cmp} in the bilayer. The binding energy is slightly increased in the bulk and varies between 93 eV and 127 meV. These numbers also compare to the binding in graphite[42] (100 eV using vdW-DF1).

The top panel of Fig. 4 presents the overall band dia-

gram for the A_+A_+ stacked graphane BL at the binding separation predicted by vdW-DF2. Corresponding band diagrams at vdW-DF1 or vdW-DF1-CO_x binding separations are qualitatively similar. Apart from the fact that each band occurs as a pair of bands, the band structure also agrees qualitatively with that of the ML (see, for example, Ref. 12).

The bottom panel of Fig. 4 summarizes some differences between the BL (bulk) and the ML, documenting the changes occurring in the k-dependent band gap with the BL (bulk) formation. We plot the differences $\Delta E_{\rm gap}^{\rm BL/bulk}(k) = E_{\rm gap}^{\rm BL/bulk}(k) - E_{\rm gap}^{\rm ML}(k)$ along $\overline{\rm K\Gamma}$, $\overline{\Gamma\rm M}$, and $\overline{\rm MK}$. In addition, for the bulk, we also plot $\Delta E_{\rm gap}^{\rm bulk}(k) = E_{\rm gap}^{\rm bulk}(k') - E_{\rm gap}^{\rm ML}(k)$. Here, k' is along $\overline{\rm HA}$, $\overline{\rm AL}$, and $\overline{\rm LH}$ in the bulk; k is the corresponding k point along $\overline{\rm K\Gamma}$, $\overline{\Gamma\rm M}$, and $\overline{\rm MK}$ in the ML (and therefore $k_x = k'_x$, $k_y = k'_y$, while $k_z = 0$ and $k'_z = 1/2$). A summary of the numerical values of band gaps at the special points (calculated with various choices of vdW-DF and corresponding BL binding separations or bulk lattice constants c) and their deviations from the corresponding values in the ML is given in Table I.

We find large vdW-induced modifications of the band structure, summerized by the k-dependent band-gap differences. In the BL, the direct band gap can deviate by up to ~ 0.8 eV (between K and Γ) with respect to the ML gap (see bottom panel of Fig. 4). In the bulk, deviations can be as large ~ -1.2 eV ($\sim +4$ eV) in some regions of the Brillouin zone (BZ) near the H point (A point).

V. DISCUSSIONS: BILAYER GRAPHANE

Our results for BL graphane suggest that vdW forces can have non-negligible effects on the the overall band structure in layered or macromolecular materials. Focusing on the direct band gap in graphane, we find modifications that are strongly k-dependent. At the K and M points (and in other regions), the modifications are significant. At the Γ point, where the gap is smallest in the ML (and in the BL), no modifications occur, rendering the BL system electronically similar to the ML system. Nevertheless, qualitative understanding of the origin of the different modifications in the various regions is important to gain further insight into the relevance of vdW interactions for materials band structure.

In the following, we explore the origin of band-gap modifications in BL graphane. We study the significance of three geometry-induced effects: (1) the charge enhancement between the ML fragments in the BL, see left panel of Fig. 1, (2) the hybridization of wave functions (WF), and (3) the charge rearrangements upon self-consistency (on the GGA-level), see right panel of Fig. 1.

We argue that the observed modifications in BL graphane can be interpreted as a concerted interplay between the occurrence of bonding-type hybridization of unoccupied WF and the electrostatic interaction between these hybridization WF and the enhanced charge density. The hybridization generally lowers the energy. The modification of electrostatic interaction can either counteract or strengthen this energy gain, depending on the nature of the hybridization WF. Our interpretation of this concerted interplay explains why the band-gap variation is modified at (and around) the K point, but not at (and around) the Γ point.

A. Band-origin of gap reduction

In the mid-panel of Fig. 5(a), we show that the main contribution to the observed band-gap variation comes from the lower conduction-band (LCB). We plot the variations of the upper valence-band (UVB) energies (dashed dark curve) and of the LCB energies (dashed light curve),

$$\Delta E_{\rm XXX}(k) = \left(E_{\rm XXX}^{\rm BL}(k) - E_{\rm F}^{\rm BL}\right) - \left(E_{\rm XXX}^{\rm ML}(k) - E_{\rm F}^{\rm ML}\right). \quad (4)$$

Here $E_{\rm XXX}^{\rm BL/ML}(k)$ is the energy of the highest (occupied) valence band (XXX = UVB) or the energy of the lowest (unoccupied) conduction band (XXX=LCB) at k in the BL/ML and $E_{\rm F}^{\rm BL/ML}$ is the Fermi level in the BL/ML. (The Fermi level is here defined by the energy of the highest occupied state).

We find that $|\Delta E_{\rm LCB}(k)|$ is typically much larger than $|\Delta E_{\rm UVB}(k)|$. This applies in particular in those regions where $|\Delta E_{\rm gap}(k)|$ is large. Thus, we assign the modifications of the band-gap variation in the BL primarily to the modifications in the LCB energy variation.

B. Hybridization in the valence band

We begin by characterizing the small effects that are found to originate from hybridizations in the VB.

The bottom panel of Fig. 5(a) shows, that the small bumps in the UVB energy variation (difference) are due to hybridization of UVB wave functions (WF). Typically the BL VB pair bands coincide with each other and with the original ML band. However, in between the K and the Γ point and in between the Γ and the M point, the UVB bands split (symmetrically) into a bonding and antibonding pair. As a result, the highest occupied states are shifted towards the Fermi level, but the magnitude of this upward shift is small ($\Delta E_{\rm UVB} < 0.25$eV), see mid-panel of Fig. 5(a). In lower-lying VB, considerably larger shifts arise around the Γ point. However, since these shifts are symmetrically positive and negative, the associated hybridization of wave functions is not a signature of bonding. Also, they do not affect any band gap.

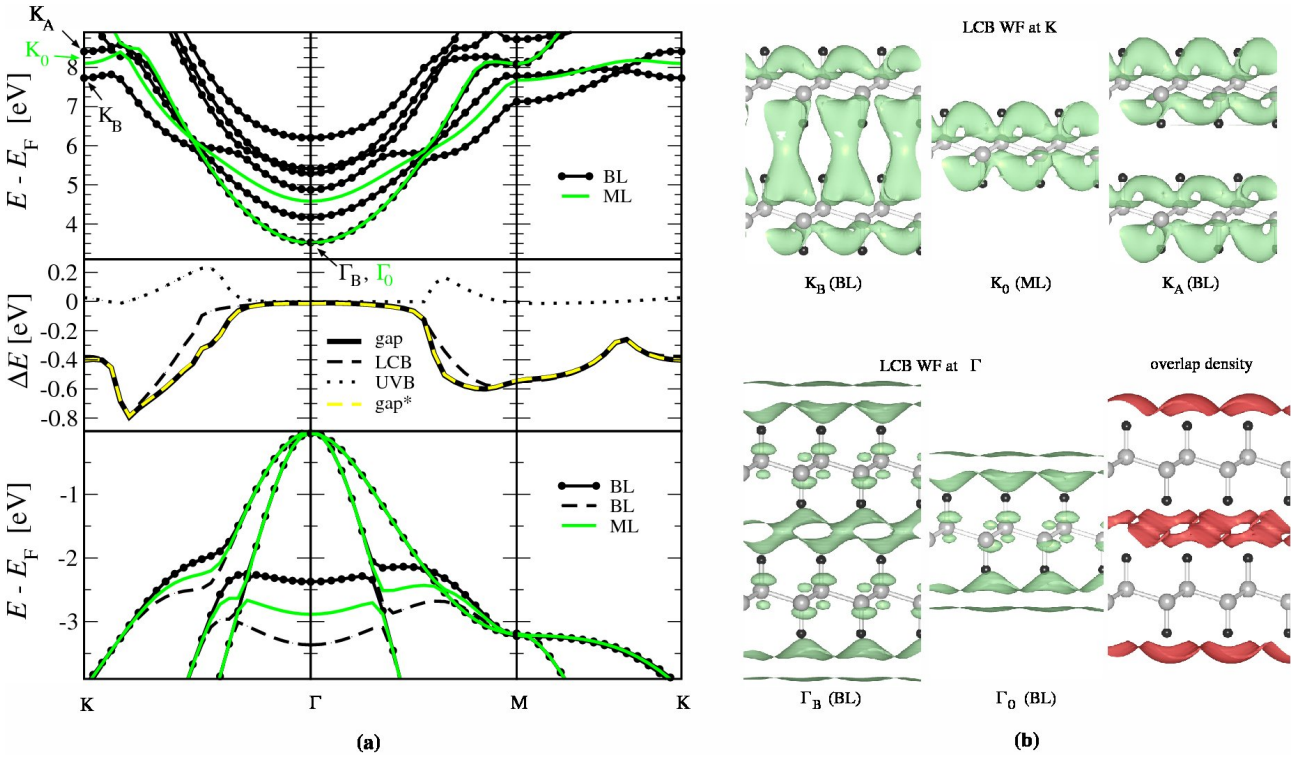

FIG. 5: (Color) Contributions to band-gap reduction and individual Kohn-Sham wave functions (WF) in vdW bonded graphane bilayers (BL). **(a)** The set of left panels compares the band structure of the BL with that of the monolayer (ML). The top (bottom) panel shows a selection of lower conduction bands (LCB) [upper valence bands (UVB)]. ML bands are represented by green lines, BL bands by black lines. Bonding and antibonding states are discriminated by solid and dashed lines. The mid panel shows the variation of direct band-gap differences between the BL and ML (solid black), the variation of UVB energy differences (dotted black), and the variation of LCB energy differences (dashed black). We also show the variation of band-gap differences calculated from the non-selfconsistent BL charge density obtained by adding two ML densities (dashed yellow). **(b)** The set of right panels shows individual LCB WFs at the K and at the Γ point. At the K point (set of top panels) the two lowest CB WF associated with the BL are essentially the bonding and antibonding combinations of the lowest CB WF located on the two MLs. This explains the decrease in the direct band gap at K. At the Γ point, the lowest CB WF in the BL (bottom left) is also essentially the bonding combination of two lowest CB WF in the ML (bottom middle); however, without energy gain. Qualitatively, this is explained by the nature of the hybrid WF and reflects the formation of a density overlap between the two ML sheets (bottom right panel). See text for a detailed analysis.

C. Self-consistent charge rearrangements

In the mid-panel of Fig. 5(a) we also show that SC charge rearrangements (on the GGA level) have no significant effect on the band gap. We contrast the band-gap variations obtained from the SC BL density (gap, black solid) and from the nSC superposition of ML densities (gap*, yellow dashed). At the displayed resolution, the curves cannot be distinguished. We find that the differences between both band-gap variations are at the meV level. Thus, the charge rearrangements[43] shown in Fig. 1 do not appreciably contribute to the band-gap variation. In fact, this also applies for the overall band structure variation.

Further charge rearrangements[5] that are inherent to vdW forces (and require a SC vdW-DF calculations)[5,44,45] are expected to be even smaller than those resulting at the the GGA level. The inherent rearrangements is not expected to be importance for the band structure. This justifies our use of nSC vdW-DF in this study of bilayer graphane.

D. Conduction-band modifications

The top panel of Fig. 5(a) shows that, in the CB, the bands for the BL system are generally not degenerate and the splitting is large at high-symmetry points. We do not interpret and discriminate the individual bands of the CB solely according to bonding and antibonding bands. Instead, we provide an analysis based on the wave functions (WF) at individual k points. We show that unoccupied WFs form bonding-type WFs both in K and Γ. To deepen our understanding of why this leads to a reduced band gap in K but not in Γ, we also analyze the overlap between the hybrid WFs with the total charge density.

The set of top panels of Fig. 5(b) details individual WFs associated with the BL and ML at K. The ML WF (K_0) is shown the middle. The left and right panels show that the BL WFs can be interpreted as bonding-type (left panel, K_B) and antibonding-type (right panel, K_A) hybridizations of the ML WF, respectively. The bottom left and mid-panel of Fig. 5(b) focus on the WFs at the Γ point. The ML WF (Γ_0) is shown in the mid-panel. The lowest-lying BL WF (Γ_B, left panel) can be interpreted as the bonding-type hybridization of two ML WFs.

Since the band gap at the Γ and K point is determined solely by the respective CB WFs (all other effects are negligible there), and since in both points, the lowest unoccupied WF is a bonding-type hybridization of two ML WFs, we would expect that the band gap is decreased in both cases. However, while this is indeed the case at the K point, the formation of the bonding-type orbital at the Γ point does not result into a lowering of energy.

E. Concerted action of hybridization and charge enhancement

We analyze the difference between the gap behavior at the K and the Γ point by comparing the overlap between the hybridization WFs and the BL charge density with the overlap between the ML WF and the ML charge density.

The bottom right panel of Fig. 5(b) shows a relevant contour of the nSC charge density of the two MLs. The LCB WF in Γ has a high weight exactly in the region where the overlap density is large. This is energetically unfavorable and may compensate for the energy gain due to hybridization. In the K point, the bonding-type hybridization WF is more smeared out, also having weight in regions where the density vanishes.

We perform a more quantitative analysis by defining the overlap between the total density $n^{\mathrm{BL/ML}}(r)$ (normalized to the number of electrons) and the partial density $n^{\mathrm{BL/ML}}_{k,\mathrm{LCB}}(r)$ associated with the lowest CB WF at k (normalized to one),

$$\mathcal{O}^{\mathrm{BL/ML}}_{k,\mathrm{LCB}} = \int d^3r \; n^{\mathrm{BL/ML}}_{k,\mathrm{LCB}}(r) n^{\mathrm{BL/ML}}(r). \qquad (5)$$

We then calculate the difference between the the overlap in the BL and (twice) the overlap in the ML,

$$\Delta\mathcal{O}_{k,\mathrm{LCB}} = \mathcal{O}^{\mathrm{BL}}_{k,\mathrm{LCB}} - 2\mathcal{O}^{\mathrm{ML}}_{k,\mathrm{LCB}}. \qquad (6)$$

A positive (negative) value of $\Delta\mathcal{O}_{k,\mathrm{LCB}}$ specifies that the overlap between the LCB WF with the total charge density is larger (smaller) in the BL than in the ML. A positive (negative) value therefore indicates a increased (decreased) electrostatic repulsion resulting into increased (decreased) energy eigenvalue of the corresponding BL WF with respect to the ML WF.

Table II summarizes the calculated values of $\Delta\mathcal{O}_{k,\mathrm{LCB}}$ using the SC and the nSC BL density. We observe that the values of $\Delta\mathcal{O}_{k,\mathrm{LCB}}$ are insensitive to whether we use the SC density or the nSC density. This is consistent with our previous observation that the charge rearrangements upon selfconsistency, are without significance for the overlap and thus for the band gap.

	$\Delta\mathcal{O}_{\mathrm{K,\ LCB}}$ [e^2/cell]	$\Delta\mathcal{O}_{\Gamma,\ \mathrm{LCB}}$ [e^2/cell]
SC	$-7.21 \cdot 10^{-4}$	$+13.61 \cdot 10^{-4}$
nSC	$-7.19 \cdot 10^{-4}$	$+13.35 \cdot 10^{-4}$

TABLE II: Difference in overlap integrals K and at Γ between the partial density associated with the LCB WF and the total selfconsistent (SC) and non-selfconsistent (nSC) density, see Eq. (6).

More importantly, we note that the different signs and magnitudes of the calculated $\Delta\mathcal{O}_{k,\mathrm{LCB}}$ at K and Γ qualitatively explain why the gap is reduced at K but not at Γ. At K, we find $\Delta\mathcal{O}_{\mathrm{K,\ LCB}} < 0$. Thus, the energy level of the BL LCB WF at K is pulled towards the VB due the concerted action of hybridization *and* of the decreased electrostatic interaction. At the Γ point, on the other hand, we find $\Delta\mathcal{O}_{\Gamma,\mathrm{LCB}} > 0$. The increased electrostatic interaction counteracts the energy gain obtained by the bonding hybridization.

VI. DISCUSSIONS: BULK GRAPHANE

In the bulk, the deviations in the band-gap variations can be considerably larger than those in the BL, see bottom panel of Fig. 4. Here, we give a more detailed analysis of the overall band structure effects associated with graphane assembly into bulk.

In the the left panel of Fig. 6, we show the band diagram along $\overline{\mathrm{K\Gamma}}$, $\overline{\Gamma\mathrm{M}}$, and $\overline{\mathrm{MK}}$. Focusing on the CB, the bulk band structure is very different from that of the BL along the same path, see top panel of Fig. 4. In particular at the Γ point, that gap is approximately twice as large as in the BL. Also, the band energy at K is considerably higher than in the BL. Only at M, we find similar band energies. Thus, the effect of vdW-bonding on local features of the band structure and related observable properties can be dramatic.

In the mid-panel of Fig. 6, we show show the band diagram along $\overline{\mathrm{HA}}$, $\overline{\mathrm{AL}}$, and $\overline{\mathrm{LH}}$. Again, the the bulk band structure is very different from that of the BL along the parallel path along $\overline{\mathrm{K\Gamma}}$, $\overline{\Gamma\mathrm{M}}$, and $\overline{\mathrm{MK}}$. The band energy at H is lower than at L, while it is the other way around at K and at M in the BL. Only around the A point (corresponding to Γ in the BL and ML cases) do the bulk and ML band diagram show similar features.

In the right panel of Fig. 6, we effectively combine the two diagrams from the left and mid-panel, calculating the band diagram for a would-be 2-layer unit cell at $k_z = 0$. The resulting band diagram shows the features of the BL band diagram and of the VB there is also a very good quantitative agreement. Therefore, the BL

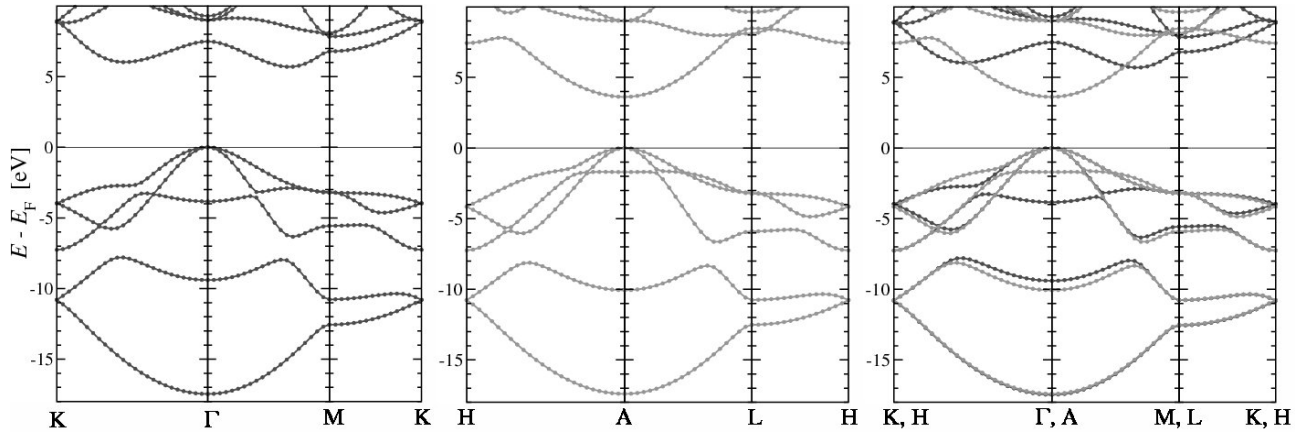

FIG. 6: Band diagrams for bulk graphane. The left panel shows the band diagram along the same path in k space as shown for the bilayer in the top panel of Fig. 4. The midpanel shows the band diagram along a parallel path in k space with $k_z = 1/2$. In the right panel we combine both band diagrams into one plot and reproduce a band diagram that possess essentially all features that are present in the BL band diagram, compare top panel of Fig. 4.

band-diagram can partly be understood as a zone-folded version of the bulk band-diagram.

VII. SUMMARY AND CONCLUSION

This paper predicts and characterizes band-structure modifications produced by pure dispersive binding between two macromolecules in possible new material systems: bilayer and bulk graphane.[15,16] Using nonselfconsistent vdW-DF calculations,[4,5,9–11] we determine the binding separation (c-lattice parameter) and binding energies in vdW-bonded graphane bilayers (bulk). We use the calculated separations to obtain corresponding GGA-DFT band diagrams. Our results demonstrate that vdW interactions can significantly alter electronic behavior, at least locally in the Brillouin zone. In graphane, the direct band gap is reduced (increased) by up to 1.2 eV (4 eV), signaling a potential to exploit dispersive interactions also in band-gap engineering.

Our analysis shows that the origin of the band-gap modifications in this system is the concerted action of two geometry-induced effects. The first cause is the (bonding-type) hybridization between *unoccupied* wave functions in the lowest conduction band. This effect generally leads to lower energy state. The second cause is the modification of the electrostatic interaction between this hybrid wave function and the total density. The cause can either strengthen or compensate for the energy gain in a bonding-type hybridization. We also find that selfconsistent charge rearrangements (on the GGA level) with respect to the ML density have no significant impact on the bandstructure. Additional charge rearrangements described by self-consistent vdW-DF calculations[5] are expected to be even smaller, justifying our use of nonselfconsistent vdW-DF.

The nature of conduction and optical absorption in BL graphane would be determined by the region around the Γ point. There, the band structure of the bilayer essentially coincides with that of the monolayer. Therefore, we expect graphane multilayers to behave electronically similar to a graphane monolayer, at least for properties defined by a simple response. For bulk graphane, the behavior is more complicated. We emphasize that other vdW-bonded systems may exist where significant band-gap modifications arise at Brillouin-zone points having higher relevance for the electronic nature of the material.

Acknowledgment

We thank G. D. Mahan for encouragement and discussions. Support by the Swedish National Graduate School in Materials Science (NFSM), the Swedish Research Council (VR), the Swedish Governmental Agency for Innovation Systems (VINNOVA) and the Swedish National Infrastructure for Computing (SNIC) is gratefully acknowledged.

* Electronic address: rohrer@chalmers.se

[1] F. Capasso, *Science* **235**, 172 (1987); F. Capasso, *Thin Solid Films* **216**, 59 (1992).
[2] V. H. Crespi, M. L. Cohen and A. Rubio, *Phys. Rev. Lett.* **79**, 2093 (1997).
[3] B. Xu and B. C. Pan, *Phys. Rev.* B *74*, 245402 (2006).
[4] D.C. Langreth, B.I. Lundqvist, S.D. Chakarova-Käck, V.R. Cooper, M. Dion, P. Hyldgaard, A. Kelkkanen, J. Kleis, Lingzhu Kong, Shen Li, P.G. Moses, E. Murray, A. Puzder, H. Rydberg, E. Schröder, and T. Thonhauser, *J.*

Phys.: Condensed Matter **21**, 084203 (2009).
[5] T. Thonhauser, V. R. Cooper, S. Li, A. Puzder, P. Hyldgaard, and D. C. Langreth *Phys. Rev.* B **76**, 125112 (2007).
[6] E. Londero and E. Schröder, Preprint arXiv:1006.2494 In press, *Phys. Rev.* B (2010).
[7] K Berland, T.L. Einstein, and P. Hyldgaard *Phys. Rev. B* **80**, 155431 (2009).
[8] G. Pawin, K. L. Wong, K.-Y. Kwon, L. Bartels, *Science* **313**, 961 (2006).
[9] M. Dion, H. Rydberg, E. Schröder, D. C. Langreth, and B. I. Lundqvist, *Phys. Rev. Lett.* **92**, 246401 (2004).
[10] K. Lee, É. D. Murray, L. Kong, B. I. Lundqvist, and D. C. Langreth, *Phys. Rev.* B 82, 081101(R) (2010).
[11] V. R. Cooper, *Phys. Rev.* B **81**, 161104(R) (2010).
[12] J. O. Sofo, A. S. Chaudhari and G. D. Barber, *Phys. Rev.* B **75**, 153401 (2007).
[13] D. C. Elias, R. R. Nair, T. M. G. Mohiuddin, S. V. Morozov, P. Blake, M. P. Halsall, A. C. Ferrari, D. W. Boukhvalov, M. I. Katsnelson, A. K. Geim, and K. S. Novoselov, *Science* **323**, 5914 (2009).
[14] K. S. Novoselov, A. K. Geim, S. V. Morozov, D. Jiang, Y. Zhang, S. V. Dubonos, I. V. Grigorieva, and A. A. Firsov, *Science* **306**, 666 (2004).
[15] O. Leenaerts, B. Partoens, and F. M. Peeters, *Phys. Rev. B* **80**, 245422 (2009).
[16] V. I. Artyukhov and L. A. Chernozatonskii, *J. Phys. Chem. A* **114**, 5389 (2010).
[17] A. K. Geim and K. S. Novoselov, *Nature Materials* **6**, 183 (2007).
[18] A. K. Geim, *Science* **324**, 1530 (2009).
[19] G. Henkelman, A. Arnaldsson, and H. Jónsson, *Comput. Mater. Sci.* **36**, 254 (2006)
[20] K. Berland, Ø. Borck, and P. Hyldgaard, submitted to *Comp. Phys. Comm.*, see also arXiv:1007.3305v1; Ø. Borck, unpublished.
[21] M. Y. Han, B. Özyilmaz, Y. Zhang, and P. Kim, *Phys. Rev. Lett.* **98**, 206805 (2007).
[22] V. Barone, O. Hod, and G. E. Scuseria, *Nano Lett.* **6**, 2748 (2006).
[23] Schedin et al. Nat. Mater. **6**, 652 (2007).
[24] M. Klintenberg, S. Lebégue, M. I. Katsnelson, and O. Eriksson, *Phys. Rev.* B 81, 085433 (2010).
[25] L. Hedin, *Phys. Rev.* **139**, A796 (1965); F. Aryasetiawan and O. Gunnarsson, *Rep. Prog. Phys.* **61**, 237 (1998).
[26] S. Lebegue, M. Klintenberg, O. Eriksson, and M.I. Katsnelson, *Phys. Rev.* B **79** 245117 (2009).
[27] A. K. Singh, E. S. Penev and B. I. Yakobson, *ACS Nano* **4**, 3510 (2010).
[28] A. K. Singh and B. I. Yakobson, *Nano Lett.* **9**, 1540 (2009).
[29] G. Savini, A. C. Ferrari, and F. Giustino, *Phys. Rev. Lett.* **105**, 037002 (2010).
[30] D. Vanderbilt, *Phys. Rev. B* **41**, 7892 (1990).
[31] B. Hammer, O. H. Nielsen, J. J. Mortensen, L. Bengtsson, L.B. Hansen, A. C. E. Madsen, Y. Morikawa, T. Bligaard, A. Christensen, and J. Rossmeisl, available from https://wiki.fysik.dtu.dk/dacapo.
[32] J. P. Perdew, K. Burke, and M. Ernzerhof, *Phys. Rev. Lett.* **77**, 3865 (1996).
[33] H. J. Monkhorst and J. D. Pack, *Phys. Rev. B* **13**, 5188 (1976).
[34] Y. Zhang and W. Yang, *Phys. Rev. Lett.* **80**, 890 (1998).
[35] E. D. Murray, K. Lee, and D. C. Langreth, *J. Chem. Theory Comput.* **5**, 2754 (2009).
[36] S.H. Vosko, L. Wilk, M. Nusair, *Can. J. Phys.* **58**, 1200 (1980).
[37] E. Ziambaras, J. Kleis, E. Schröder, and P. Hyldgaard, Phys. Rev. B 76, 155425 (2007).
[38] S. D. Chakarova-Käck, E. Schröder, B. I. Lundqvist, and D. C. Langreth, *Phys. Rev. Lett.* **96**, 146107 (2006).
[39] K. Johnston, J. Kleis, B. I. Lundqvist, and R. M. Nieminen, *Phys. Rev. B* **77**, 121404(R) (2008).
[40] J. Kleis, E. Schröder, and P. Hyldgaard, *Phys. Rev. B* **77**, 205422 (2008).
[41] H. Ibach and H. Lüth, *Solid-State Physics: An Introduction to Principles of Materials Science* 3rd ed. (Springer-Verlag 2002).
[42] S. D. Chakarova-Käck, A. Vojvodic, J. Kleis, P. Hyldgaard, and E. Schröder, *New J. Phys.* **12** 013017 (2010).
[43] In the present case the charge rearrangements are not accompanied by any significant charge transfer. Our Bader analysis[19,20] shows that the difference in charge before and after the charge rearrangement is $\Delta q \leq 5 \cdot 10^{-4}$ e/atom. In cases where charge transfer takes place, see for example Ref. 6, such rearrangements may have more significance.
[44] G. Román-Pérez and J. M. Soler, *Phys. Rev. Lett.* **103**, 096102 (2009).
[45] Selfconsistent vdW-DF is available in the opensource code GPAW,[46] see *https://wiki.fysik.dtu.dk/gpaw/index.html.*
[46] J. Enkovaara, C. Rostgaard, J. J. Mortensen et al. *J. Phys.: Condens. Matter* **22**, 253202 (2010).